Delft University of Technology

Conceptual design of compliant bone scaffolds by full-scale topology optimization

Smit, Thijs; Koppen, Stijn; Ferguson, Stephen J.; Helgason, Benedikt

Important note
To cite this publication, please use the final published version (if applicable).
Please check the document version above.

Conceptual design of compliant bone scaffolds by full-scale topology optimization

Thijs Smit [a,*], Stijn Koppen [b], Stephen J. Ferguson [a], Benedikt Helgason [a]

[a] *Institute for Biomechanics, ETH-Zürich, Zürich, Switzerland*
[b] *Department of Precision and Microsystems Engineering, Delft University of Technology, Delft, the Netherlands*

A B S T R A C T

A promising new treatment for large and complex bone defects is to implant specifically designed and additively manufactured synthetic bone scaffolds. Optimizing the scaffold design can potentially improve bone in-growth and prevent under- and over-loading of the adjacent tissue. This study aims to optimize synthetic bone scaffolds over multiple-length scales using the full-scale topology optimization approach, and to assess the effectiveness of this approach as an alternative to the currently used mono- and multi-scale optimization approaches for orthopaedic applications. We present a topology optimization formulation, which is matching the scaffold's mechanical properties to the surrounding tissue in compression. The scaffold's porous structure is tuneable to achieve the desired morphological properties to enhance bone in-growth. The proposed approach is demonstrated in-silico, using PEEK, cortical bone and titanium material properties in a 2D parameter study and on 3D designs. Full-scale topology optimization indicates a design improvement of 81% compared to the multi-scale approach. Furthermore, 3D designs for PEEK and titanium are additively manufactured to test the applicability of the method. With further development, the full-scale topology optimization approach is anticipated to offer a more effective alternative for optimizing orthopaedic structures compared to the currently used multi-scale methods.

1. Introduction

Critically Sized Bone Defects (CSBDs) are defects too large to heal spontaneously. They are often the result of tumour removal surgery or trauma. Traditionally, CSBDs are treated using autologous bone graft, which facilitates bone growth and can be used in combination with a fixation plate to stabilize the treated domain (Kelly et al., 2021). Using autologous bone graft is considered the gold standard in treating CSBDs, but the amount of available bone graft material is limited when harvested from the patient's own body (Pobloth et al., 2018). Furthermore, post-operative donor-site morbidity and infections can occur which may result in revision surgeries. Therefore, alternative treatments are sought to improve patient care and decrease health-care costs (Wang et al., 2016; Metz et al., 2020).

A promising alternative treatment, to avoid or to reduce the need for autologous bone graft, is to implant a specifically designed and manufactured Synthetic Bone Scaffold (SBS) (Egan et al., 2019; Barba et al., 2019). The SBS should provide mechanical and biological conditions which enhance bone formation and bridging of the CSBD through

natural bone growth into the SBS (Hollister, 2009). To facilitate bone in-growth, the SBS should be a porous structure (a material containing voids) made of a bio-compatible material. Autologous bone graft is only load bearing to a limited extent, however SBSs can be fully load bearing and provide mechanical stability to the treated domain. Therefore, SBSs have the potential to aid healing CSBDs or to be used in other orthopaedic applications (Vidal et al., 2020; Mobbs et al., 2017). An overview over current clinical applications of bone scaffold can be found in *e.g.* (Mittwede et al., 2018).

The bone growth rate into SBSs and peri-implant bone remodelling are influenced by the scaffold's mechanical and morphological properties like elastic modulus, porosity, pore size and permeability (Hollister, 2009; Egan et al., 2017). The primary function of the SBS is to provide mechanical stability to the treated domain. However, the SBS potentially causes under-loading (stress-shielding) or over-loading (subsidence or fracture) of the adjacent bone structures, as a result of the mismatch in mechanical properties between the implant and the adjacent tissue (Wang et al., 2016). This was emphasized by Bahraminasab et al. who identified the current challenges of bone scaffolds for clinical

application (Bahraminasab, 2020). They concluded that the scaffold should provide sufficient mechanical stability and appropriate stiffness, similar to the stiffness of bone at the defect site, to allow for natural bone remodelling.

Tailored SBS design can improve the scaffold's ability to promote bone in-growth (Rubert et al., 2021), although, the design requirements are conflicting each other. For example, decreasing the scaffold's apparent stiffness by increasing porosity might results in a strut diameter which is too small for manufacturing. Therefore, the optimal SBS design is a trade-off between mechanical, morphological, and manufacturing requirements. The trade-off in the design of SBSs advocates for the use of optimization tools in the design process.

Topology optimization (TO) is a numerical method to find the optimal lay-out of a structure within a specific domain (Sigmund and Bendsøe, 2004). In orthopaedic applications, various TO formulations have been used (Metz et al., 2020; Hollister et al., 2002; Al-Tamimi et al., 2017; Moussa et al., 2020; Sutradhar et al., 2010). Several studies used to design scaffolds and implants with the goal of maximizing bone formation using mechano-biological models or bone-growth models in the optimization loop (Wu et al., 2020). These TO approaches result in mono-scale structures, *i.e.* structures that are produced with the classic form of TO with material clustering to create structures on a single length-scale. Consequently, designing structures on the scale of the bone defect, the macro-scale, would not allow the creation of pores in the preferred pore size range on the meso-scale. Although, the mono-scale approach produces high performing designs (Wu et al., 2021), the designs are non-porous and therefore the mono-scale approach is not suitable for designing SBSs or other orthopaedic structures requiring bone in-growth.

Other previous efforts to optimize SBSs with computational tools rely on multi-scale methods where a design can be optimized over two length-scales, if the length-scales are sufficiently separated. The macro-scale structure is often constructed by periodically repeating a micro-scale unit-cell, *e.g.*, in lattice structures. Structural optimization can be applied to both scales (Milovanović et al., Vitković; Zadpoor, 2019; Garner et al., 2022; Boccaccio et al., 2016; Cohen et al., 2021). The use of the multi-scale approach in optimization of SBSs is motivated by the possibility to design porous structures with limited computational effort (Wu et al., 2021). Furthermore, manufacturable designs can be produced efficiently, because, for a variety of unit-cells, the design is manufacturable when the unit-cell is. Furthermore, the mechanical and biological characteristics of the scaffold can be optimized by changing the unit-cell properties.

The disadvantage of using the multi-scale methods is that it results in sub-optimal designs (a sub-optimal design refers to a design that is not the best possible solution for a given problem), because restrictions are enforced on the solution space. In many cases, these restrictions come from prescribing the unit-cell topology and therefore part of the design freedom is eliminated (Wu et al., 2021; Groen et al., 2021). Furthermore, non-smooth transitions between unit-cells arise when unit-cells with different strut sizes are used (Garner et al., 2019), and finally, optimization using the multi-scale approach is based on the assumption that the two scales of interest are sufficiently separated. If this is not the case, *e.g.*, due to manufacturability considerations, the 'scale effect' will play a dominant role leading to sub-optimal designs (Zhang and Sun, 2006; Wu et al., 2019). In the case of SBSs, the macro-scale is defined by the scale of the CSBD and will typically range from around 1 cm up to a few centimetres. The scale of the pores and struts, the meso-scale, is typically around 500 µm. Therefore, the scales of interest, when optimizing SBSs are relatively close, and we can expect sub-optimal results using multi-scale methods.

The full-scale approach is essentially a high-resolution mono-scale approach which can produce multi-scale structures (Aage et al., 2017). Pushing the designs towards a porous structure can be achieved by additional local volume constraints (Wu et al., 2021). The full-scale approach is considerably different from the multi-scale approaches for orthopaedic applications. The advantage is that tuneable porous structures are generated, suitable for bone in-growth. Furthermore, connectivity issues are naturally solved and the assumption of separation of length-scales is not used. This means that the full-scale approach can effectively optimize over two length-scales which are not sufficiently separated.

The aim of this study is to investigate the application of full-scale to design SBSs with tuneable mechanical and morphological properties, and to evaluate this approach as an alternative to the currently used multi-scale optimization approaches for orthopaedic applications. We hypothesize that a full-scale TO approach yields better performing SBS designs compared to the multi-scale optimization methods.

2. Materials and methods

The TO formulation in this work follows the density approach using a linear elastic Finite Element (FE) model, assuming small displacements and a linear stress-strain relationship. The computational domain is discretized with 4-node quadrilateral and 8-node hexahedron finite elements, in 2D and 3D respectively. The Solid Isotropic Material with Penalisation method (SIMP) is used to enable convergence to a solid-void design (Sigmund and Bendsøe, 2004). The Method of Moving Asymptotes (MMA) is used as an optimizer (Svanberg, 1987). A density filter is applied to avoid numerical artifacts (Bourdin, 2001). A design variable $x_i \in \mathbb{X} := \{x \in \mathbb{R} \quad | \quad 0 \leq x \leq 1\}$ is assigned to each element in the design domain with $i = 1...n$ and n the number of elements in the design domain.

2.1. Full-scale topology optimization

The full-scale approach is implemented using a large-scale TO framework which is capable of designing structures with high-resolution (Smit et al., 2021). The printing resolution of the metal powder bed fusion process of choice is roughly 25 µm. The minimum required strut diameter is 200 µm and for an accurate stress prediction we require about 8 elements through the cross-section of a strut with minimum strut diameter. Therefore, the mesh size is set to 25 µm, similar to the printing resolution of the metal powder bed fusion process of choice.

To design porous structures with tuneable porosity and pore size, the local volume constraint is used which limits the amount of material locally around each voxel (Wu et al., 2018). This leads to controllable porous structures by using; r the radius of a circular shape in 2D or a spherical shape in 3D defining the neighbourhood around each voxel and α, which defines the allowable local volume fraction in the voxel neighbourhood. A p-mean aggregation with a penalty parameter of $p = 16$ is used to convert the per-voxel constraints to one global constraint $v(x)$. Tuning of the resulting mean pore size and porosity of the final design is done by adjusting parameters r, α and p. The TO formulation to maximize stiffness with a local volume constraint is written as:

$$\min_{\mathbf{x}} u^T K u$$

$$s.t. \; v(x) \leq \alpha, \text{(Local volume constraint)},$$

$$0 \leq x_i \leq 1 \quad i = 1...n$$

where u is the displacement field and K is the stiffness matrix. This formulation, in combination with a high-resolution mesh, will be used to compare the mono-, multi- and full-scale approaches. For this comparison, the multi-scale design approach is using a "cross" and a "pore" unit-cell. The multi-scale optimization is performed according to Gao et al. (2019) using a fixed unit-cell topology.

2.2. Scaffold formulation

To maximize the SBS's stabilizing function and to address the issue of

under- and over-loading of the adjacent tissue we propose a "Scaffold" formulation, based on the work of Koppen et al. (2021). The formulation maximizes the SBS's stiffness under shear loading (variable k_s in Fig. 1a) but constrains the stiffness of the SBS in compression (variable k_c in Fig. 1a) to a patient-specific value to indirectly prevent under-loading and to prevent exhaustion of the load-bearing capacity of the adjacent bone structures. This is based on the observation that for many applications, *e.g.* in the spine, compression is a dominant daily-living load-case (Rohlmann et al., 2008). Furthermore, studies on fracture healing indicate that the compression plays a dominating role in determining tissue differentiation (Carter et al., 1988; Claes and Heigele, 1999) and finally, we found in our work that the stiffness of the SBS in shear, although maximized, depends proportionally on the target stiffness of the SBS in compression. To enhance bone in-growth, a particular pore size range between 200 μm and 1000 μm is preferred, which is experimentally obtained as best suitable pore size range for bone in-growth (Wang et al., 2016; Taniguchi et al., 2016; von Doernberg et al., 2006). Furthermore, to promote manufacturability the target minimum strut diameter is set to 200 μm (Melancon et al., 2017).

An optimization domain Ω, a square in 2D and a cube in 3D, is used with side lengths L of 8 mm. Compression (w in Fig. 1b) and shear (u in Fig. 1c) are applied in the form of displacements in the linear regime. The degrees of freedom at the bone-scaffold interface without a prescribed displacement are fixed. Strain energy U (Nm) is used as a measure of stiffness. Compression strain energy U_c is approximately related to SBS's apparent stiffness k_c (N/m) and apparent elastic modulus $E_c(N/m^2)$ by $U_c = \frac{1}{2}k_c u^2$ and $U_c = \frac{1}{2}\frac{E_c A}{L}u^2$, respectively. The "Scaffold" formulation is mathematically described as:

$$\min_{\mathbf{x}} -f(U_s(\mathbf{x}))$$

$$s.t. \ U_c(\mathbf{x}) \leq U_t,$$

$$v(\mathbf{x}) \leq \alpha, \text{(Local volume constraint)},$$

$$0 \leq x_i \leq 1 \quad i = 1 \ldots n$$

with U_t being the target strain energy which is set to be equivalent to the apparent elastic modulus of 1 GPa (Hollister, 2009). The target strain energy value can be chosen to be similar to the patient's apparent stiffness of the bone surrounding the SBSs for a patient-specific SBS design. The multi-objective function $f(U_s)$ contains the shear strain energy and U_c contains the compression strain energy. In the 3D case the strain energies of the two shear directions are included in the multi-objective function. The strain energy is defined as:

$$U_k = \frac{1}{2}u_k \cdot K(x)u_k$$

where u_k is the displacement field with k corresponding to the shear (s) or compression (c) load-cases. $K(x)$ is the stiffness matrix. This formulation, in combination with the high-resolution mesh (25 μm mesh size), will be referred to as the "Scaffold" formulation. The optimization process is terminated when the maximum design change is smaller than 10^{-3} between iteration steps or when the maximum number of iterations exceeds 1100, to limit computational time. Symmetry of the resulting design is enforced by averaging design variables over the x-, y- and z-axis. Therefore, round-off errors are avoided, but asymmetries over the diagonals are not constrained.

2.3. 2D scaffolds

2D designs are generated using the Scaffold formulation for a parameter study on the pore size, porosity, and different material properties. The parameter study is performed to get an insight into the formulation's morphological-mechanical property relationship, and to show that the morphological properties of the scaffolds are tuneable towards an optimum to facilitate bone in-growth. The designs are generated for three different porosities, *i.e.*, 60%, 70% and 80% and three different mean pore sizes, *i.e.*, 250 μm, 450 μm and 650 μm. The simulations are carried out for three different materials; PEEK, cortical bone and titanium, with E-modulus (E) of 3, 16 and 110 GPa, respectively (Wang et al., 2016; Zysset et al., 1999; Zhao et al., 2018). We choose PEEK and titanium for this study because of their relevance for orthopaedic applications. Optimization using cortical bone properties is added to the study to provide a comparison between the optimized structures and trabecular bone without the intention of manufacturing, as we are not aware of biocompatible, printable materials with bone-like mechanical properties. Other optimization parameters are provided in Table 1.

2.4. 3D scaffolds

Using the Scaffold formulation, 3D designs are generated with material properties of PEEK, cortical bone and titanium, respectively. The filter radius for the PEEK and titanium designs are increased to a radius including 6 elements to increase the strut diameter to investigate the manufacturability of the SBSs. The design with cortical bone material properties is not expected to be manufactured and therefore the standard filter radius including 2 elements is used.

The following AM processes are specifically of interest considering the manufacturing of bio-compatible, load-bearing SBSs made from commonly used materials in orthopaedics; metal powder bed fusion processes for medical grade titanium (Kelly et al., 2021; Wang et al., 2016) and Material Extrusion (MEX) AM for PEEK (Zhao et al., 2018). The titanium SBS design is manufactured using an EOS M290 machine (Ecoparts AG, Hinwil, Switzerland) with 30 μm layer height and powder
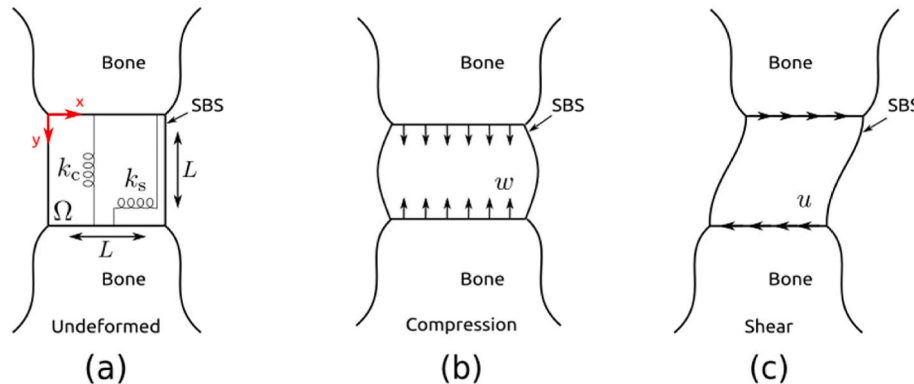

Fig. 1. 2D "Scaffold" problem definition. Domain Ω with side lengths L. Coordinate system is indicated in red. Applied displacements are indicated with w for compression and u for shear.

with an average particle size of 37 μm. No support structures are used. The PEEK design is manufactured on a Kumovis R1 machine (SINTX Technologies Inc., Salt Lake City, USA) with a nozzle size of 200 μm and a layer height of 100 μm. The PEEK design is manufactured in sizes scaled to 100%, 150%, 200% and 300%.

2.5. Post-processing of data

The resulting designs from the optimization process are called 'as-designed' and have a voxelized surface, because of the voxel-based discretization. First, a threshold operation is performed on all design variables with $x_i \geq 0.5$ set to 1.0 and the other design variables set to 0.0 to eliminate intermediate densities which may be present in the final design. Subsequently, the 'as-built' design is achieved by smoothing the voxel geometry, using vtk 9.1.0 (Schroeder et al., 1996). The 'as-built' design is used for manufacturing and FE-analysis. Morphological properties, i.e. porosity, pore interconnectivity, pore and strut diameter distributions of the 3D SBS designs, are quantified using the open-source python packages openPNM 3.1.0 (Gostick et al., 2016) and porespy 2.2.2 (Gostick et al., 2019).

For the 2D designs the ratio R between the compression strain energy of the final design and the target strain energy is quantified with $R = U_c/U_t$. This ratio quantifies how close a given design is to reaching the target stiffness of 1 GPa.

FE-analysis are performed on the 'as-built' 3D designs (Abaqus 6.14, Dassault Systèmes, Vélizy-Villacoublay, France) with the same boundary conditions as used for the optimization process. Compression and shear are applied in the form of displacements in the linear regime. Degrees of freedom at the bone-scaffold interface without a prescribed displacement are fixed. The STL models of the 'as-built' designs are meshed into a volumetric mesh (ANSA, BETA CAE Systems International AG, Root, Switzerland). The mesh consists of four-node tetrahedral elements (C3D4), with an average mesh element edge length of 0.07 mm and a mesh refinement in regions of high curvature down to a mesh element edge length of 0.002 mm. Linear elastic material properties are used to calculate the apparent elastic modulus in compression and shear.

3. Results

3.1. Comparing mono, multi, and full-scale methods

The comparison of the three different optimization approaches; the mono, multi- and full-scale in 2D is illustrated in Fig. 2. The mono-scale approach yields a column like structure with the highest performance, quantified as the objective value normalized with respect to the objective value of the mono-scale design (Fig. 2a). However, the design does not have small pores which could facilitate bone in-growth. The resulting macro-scale structural layouts of the multi-scale designs are very dependent on the choice of the unit-cell with lower performance compared to the other two approaches (Fig. 2b and 2c). The full-scale approach results in a tuneable porous structure, which is favourable
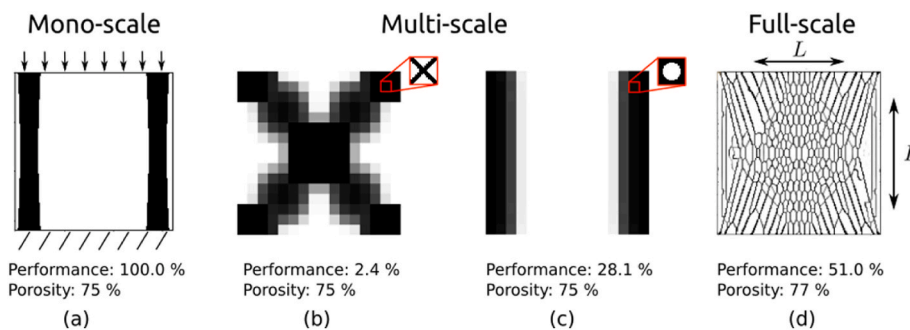
for bone in-growth (Fig. 2d). The performance measure of the full-scale design is about half compared to the mono-scale design, but about two times better than the multi-scale designs. The full-scale design is performing 81% (((51.0–28.1)/28.1) * 100%) better compared to the best performing multi-scale design.

3.2. 2D SBS designs

The results of the 2D parameter study, with varying pore diameter and porosity with the material properties of PEEK, cortical bone, and titanium, are illustrated in Figs. 3–5. "Bone-like" structures emerge, and a morphological-mechanical property relationship can be observed with increasing porosity and pore size resulting in decreasing compressive stiffness. The SBS designs with 80% porosity and smallest mean pore diameter range did not converge, because in this case there is not enough material available to the local volume constraint to create a dense network of struts. For the PEEK and cortical bone SBSs the design domain is fully utilized, and the strut diameter is constant throughout the domain. The highly porous designs made of PEEK and cortical bone have compressive stiffness which does not reach the 1 GPa target, because the local volume constraint limits the amount of material used (Figs. 3 and 4). The titanium SBS designs all reached the compressive stiffness target but have parts of the domain not utilized by a porous structure or have very small strut sizes. This is due to the high E-modulus of titanium which reduces the amount of material used in the designs.

3.3. 3D SBS designs and prototypes

The results of the morphological analysis of the resulting 3D designs for PEEK, cortical bone and titanium are illustrated in Fig. 6. Pore size distributions show that all three designs have pore sizes in the intended range between 200 μm and 1000 μm. The resulting cortical bone SBS exhibit the overall largest pores and highest porosity, while the PEEK SBS has the lowest. The design with cortical bone material properties has a "bone-like" architecture. This design does not have a minimum strut size which resulted in thinner struts throughout the design and higher porosity. Upon analysis of the pore interconnectivity, it is concluded that the cortical bone design does not have isolated pores or isolated clusters of pores. The PEEK design has 680 isolated pores on a total of 3723 pores and in the titanium design we found 2 isolated clusters of 24 pores and 4 individually isolated pores out of a total of 2540 pores. The strut size distributions show that the minimum strut size for the PEEK and titanium scaffolds of 200 μm is not fully achieved, although the majority of the struts satisfy the target minimum strut size.

The results of the FE-analysis for apparent mechanical properties of the 3D designs are provided in Table 2, together with the SBSs porosities. The apparent compressive modulus of the titanium design of 0.938 GPa compares well with the target stiffness of 1 GPa ($U_c = U_t$). Because of the smoothing operation we expect a more compliant behaviour of the 'as-built' SBSs compared to the 'as-designed' SBSs. The PEEK design has a relatively high compressive modulus of 1.488 GPa which corresponds

Fig. 2. Comparison of the 2D test problems under compression loading with a 320×320 domain and comparable material use. Boundary conditions are illustrated on the mono-scale design. The formulation is defined in section 2.1 and the performance measure is the final objective value scaled with the mono-scale design being 100%. The porosity is tuned to be similar for all test problems with $\Psi = 1 - f$, where f is the material volume fraction (**a**) final design using the mono-scale approach (**b**) macro-scale structural layout of the final design using the multi-scale approach with an enforced "cross" unit-cell. (**c**) macro-scale structural layout of the final design using the multi-scale approach with an enforced "pore" unit-cell (**d**) final design of the full-scale approach.

Mono-scale — Performance: 100.0 %, Porosity: 75 % (a)

Multi-scale — Performance: 2.4 %, Porosity: 75 % (b) — Performance: 28.1 %, Porosity: 75 % (c)

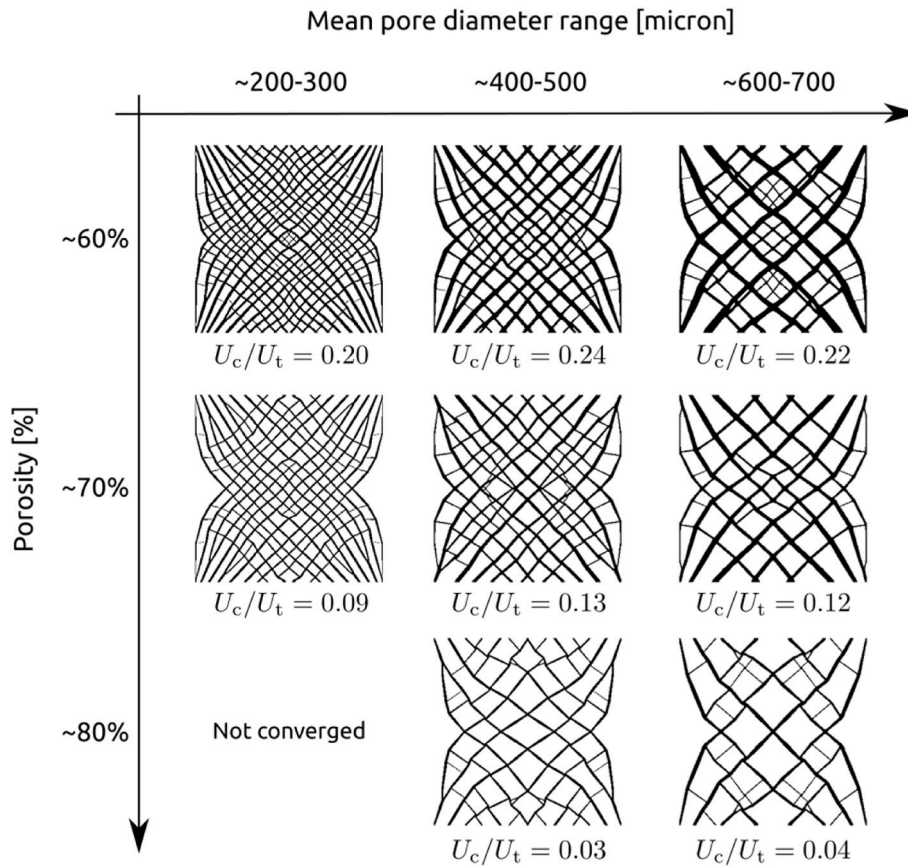**Full-scale** — Performance: 51.0 %, Porosity: 77 % (d)

Fig. 3. 2D parameter study results for PEEK ($E = 3$ GPa). The morphological-mechanical property relationship is visualized with the resulting mean pore diameter range and porosity on the x- and y-axis, respectively. The final designs are illustrated and below each design R (U_c /U_t) is provided, indicating the scaffold's compressive stiffness compared to the design target.

to a relatively low porosity of 13.1% and low mean pore size of 247.7 $\pm$ 115 μm. The cortical bone design has a compressive modulus of 0.327 GPa and relatively high porosity of 85.5% and high mean pore size of 448.8 $\pm$ 182 μm. The titanium design has a compressive modulus of 0.938 GPa and a mean pore size of 412.9 $\pm$ 202 μm.

Cross-sections of the 3D designs and additively manufactured SBSs are illustrated in Fig. 7. The internal porous structure of the titanium design consists mostly of wall-like structures and a few struts (Fig. 7a). The titanium SBS is additively manufactured successfully, although the surface finish is rough (Fig. 7b). The cortical bone design shows mostly strut-like structures and a few walls (Fig. 7c). The 3D-printed PEEK SBS of 100%, 150% and 200% scaling show inaccuracies due to the mismatch in 3D-printing resolution capabilities and the degree of detail of the design (Fig. 7d). The 300% scaled SBS shows a reasonable 3D-printed result, however, the need for scaling is indicating that the printing resolution is not sufficient for this specific application.

4. Discussion

The aim of this study was to optimize SBSs using the full-scale TO approach and to evaluate this approach as an alternative to the currently used multi-scale optimization methods for orthopaedic applications. We hypothesized that the full-scale approach yields better performing designs compared to the currently used multi-scale methods. A comparison between the approaches using a test problem showed that the mono-scale approach delivers the best performing design relatively, which is in line with results reported by Wu et al. (2021). This is expected because for the mono-scale approach the solution space is not restricted by a fixed unit-cell geometry (multi-scale) or a local volume constraint (full-scale). However, the design resulting from the mono-scale

approach is not favourable for orthopaedic applications, because it provides limited support for bone in-growth. Furthermore, we observed that the full-scale approach yields about two times better performing design than the multi-scale approach and results in a porous design which can be tuned to be favourable for bone in-growth. The comparison between the three approaches also suggests that the main drawbacks of the multi-scale approach are the dependency of the final design on the unit-cell geometry and the two scales (macro and micro) not being separated sufficiently leading to a decrease in performance. In other words, the micro-scale unit-cell is too large relative to the macro-scale scaffold structure. These observations are in line with previous reported results (Zhang and Sun, 2006). Given a fixed amount of material, the full-scale approach provides a tuneable porous structure favourable for bone in-growth with least impact on the performance of the design.

The 2D parameter study reveals trabecular bone-like structures. The similarity between the structures produced by TO and the structure of trabecular bone was realized by van Oers et al. (van Oers et al., 2008). They used an algorithm to simulate bone growth similar to a standard TO formulation. Additionally, the similarity is confirmed by studies showing that the trabecular orientation in bone is matching the principal stress directions (TAKAHASHI, 1982). We observe this in the bone-like SBS where the bone-like structures are a result of aligning the struts with the principal stress directions. Another interesting observation is that the struts are evenly spread through the design domain for the PEEK and cortical bone designs, although this is not specifically enforced in the problem definition (Figs. 3 and 4). This is favourable for the design of SBSs to support bone in-growth. For the titanium designs, parts of the design domains are not filled with struts (Fig. 5). This is due to the high E-modulus of the material which leads the optimizer to reduce the amount of material to decrease the apparent compressive stiffness of the
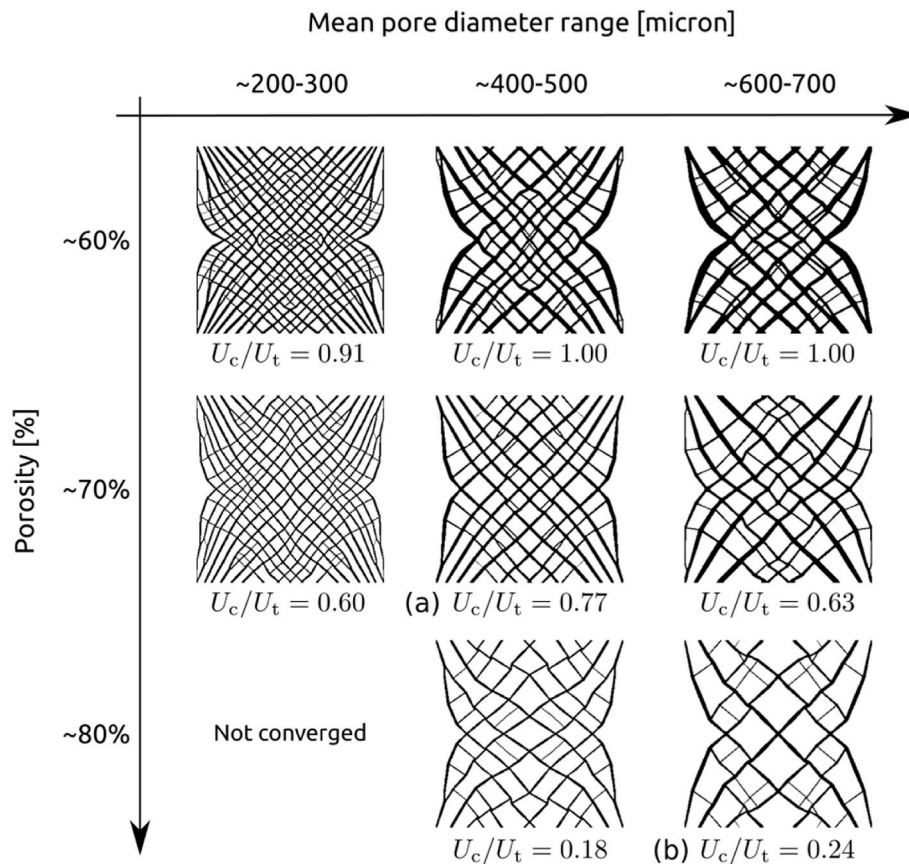
Mean pore diameter range [micron]

Fig. 4. 2D "Bone-like" scaffolds using cortical bone material properties ($E = 16$ GPa). The morphological-mechanical property relationship is visualized with the resulting mean pore diameter range and porosity on the x- and y-axis, respectively. The final designs are illustrated and below each design R (U_c /U_t) is provided, indicating the scaffold's compressive stiffness compared to the design target.

structure. Finally, the parameter study reveals a morphological-mechanical property relationship which can be used to tune the pore size and porosity of the SBS for patient-specific designs where different patients and different implant locations have different mechanical and morphological requirements.

The 3D SBS design with cortical bone material, with a compressive modulus of 326 MPa, a porosity of 85% and a mean pore size of 449 μm, reveals a morphological-mechanical property relationship which is similar to human vertebral trabecular bone. Although the specific properties of human vertebra vary widely, as an example, human vertebra properties were reported with a compressive modulus of 330 MPa, with a porosity of 94% and a mean pore size of 939 μm (Rincón-Kohli and Zysset, 2009; Zhou et al., 2014). The morphological and mechanical properties of human trabecular bone vary with anatomical site and from patient to patient. This shows the advantage of using the Scaffold formulation, because a patient-specific SBSs with desirable mechanical and morphological properties can be generated by tuning the input parameters, the target stiffness of the SBS U_t, the local volume fraction α and local volume filter radius r, respectively. Interestingly, the resulting designs are asymmetric over the x-y diagonal. We investigated the sensitivities of the objective function and the constraints and concluded that this is not due to round off errors. A fully symmetric design can be enforced, but this will additionally restrict the solution space and might reduce the performance of the design.

We observe a discrepancy between the target and resulting compressive modulus for the PEEK and cortical bone designs. The cortical bone design could not reach the target compressive modulus because adding more material was constraint (by the local volume constraint) to reach the mean pore size corresponding to human trabecular bone. This resulted in a high porosity. The high porosity was

allowed because the filter radius was kept low since no manufacturing was intended for this design. Looking at the PEEK design the compressive modulus is higher than intended. In this case the filter radius was increased to imporve the design's manufacturability (see section 2.4), which resulted in a relatively low porosity and high compressive modulus. This indicates that morphological input parameters (local volume constraint and filter radius) dominated the design outcome compared to the target stiffness input, resulting in the compressive modulus deviating from the target. This confirms our intention to be able to tune the morphological properties of the final designs, however the inputs must be chosen carefully. Additionally, we can expect a discrepancy because of the smoothing operation and the threshold operation to eliminate intermediate design variables. We intentionally modelled the SBSs without a fixation plate, in our study, in order not to confound the results, as the design of the fixation plate may depend significantly on the application (Boerckel et al., 2012).

In terms of manufacturability of the resulting structures, the final designs are clearly pushing the limits of what is manufacturable with the current state of the 3D-printing technology. Analysing the SBS prototypes produced in this study makes it clear that currently, metal powder bed fusion processes are more suitable than MEX for printing structures at the resolution we are working with. The MEX processes require higher-resolution or will require major changes in the proposed optimization methods to produce MEX compatible designs. An alternative optimization strategy that could be considered is the robust formulation for TO which can ensure a minimum strut diameter and a minimum pore size (Wang and Stefanov, 2011). Furthermore, other materials and 3D-printing technologies are available, like stereolithography, which offers higher resolution than metal powder bed fusion processes or MEX, however, this method is not commonly used for
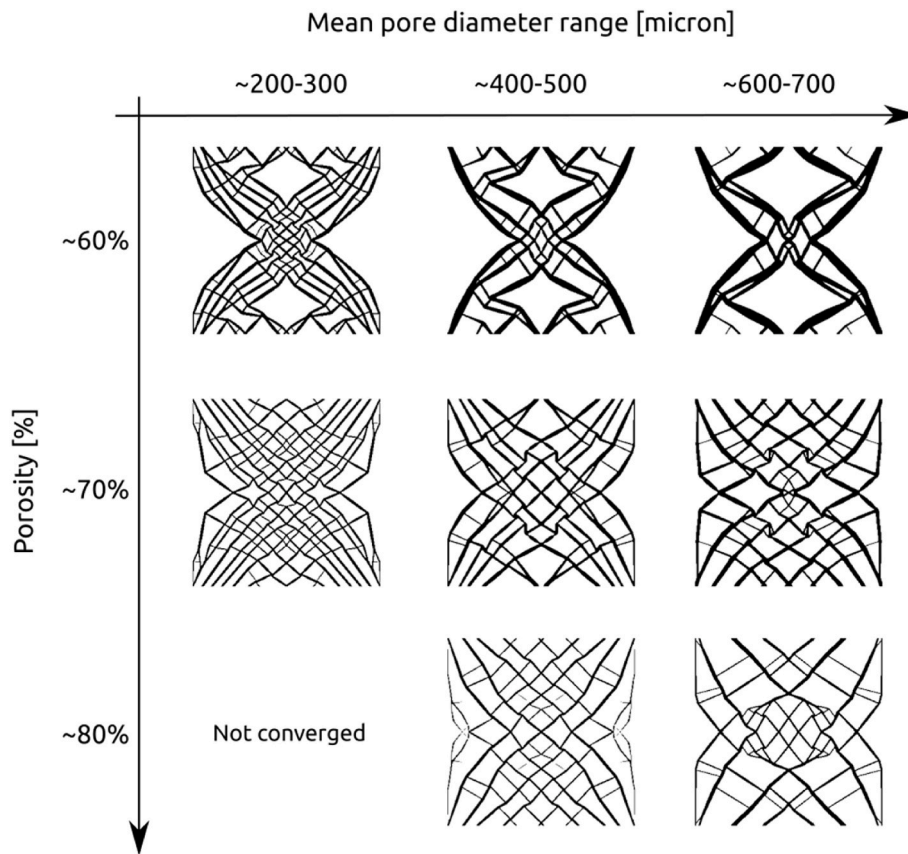
Fig. 5. 2D titanium scaffolds ($E = 110$ GPa). All have a R (U_c / U_t) ratio of 1. The morphological-mechanical property relationship is visualized with the resulting mean pore diameter range and porosity on the x- and y-axis, respectively. The final designs are illustrated.

load-bearing orthopaedic applications and is therefore not under focus in this study. The titanium design violated the target minimum strut diameter a few times (Fig. 6i). Interestingly, most of the struts with smaller strut diameter than 200 μm are 3D-printed correctly. This is in contrast to a result reported by Barba et al. (2019) who concluded a minimum strut diameter of 250 μm is required. To determine a suitable minimum strut diameter the question is how much performance loss and geometric errors are acceptable for the application. The additively manufactured titanium SBS shows both a rough surface finish and geometric errors (Fig. 7b). The rough surface finish is most likely the result of large particles in the titanium powder. Another manufacturability consideration is the interconnectivity of the pores. This is especially critical for metal powder bed fusion processes. Adding a manufacturability constraint to ensure connectivity of the pores should be considered in future work (Zhang and Cheng, 2022). Permeability is another important aspect in the design of SBSs which has been studied by multiple researchers (Guest and Pre, 2006; Du et al., 2019). Incorporating permeability in the optimization formulation could also be considered.

A limitation of using the full-scale approach, proposed in this study, is the large computational resources needed to generate a 3D design. The optimization process is run in parallel on 768 cores and took multiple days to finish. This would not be viable in a clinical setting where a patient with trauma needs an operation within a few days. In the future, computational resources might be more widely available which would make full-scale TO attractive in clinical applications *e.g.* patient-specific SBSs and implants. Alternatively, the approach could be applied to optimize the design of scaffolds and implants to fit a sub-set of the general patient population. In this case the computation time is not an issue and patients can benefit from the optimization. A second limitation associated with our study is that the test problem and the formulation to

generate 3D designs are not one-to-one comparable. Therefore, the results of the test problem should be interpreted as an indication, but the results should not be generalized. A third limitation is that the proposed method is generating designs for two specific load-cases. The variability of the load-cases in-vivo is not fully captured by the applied load-cases in this study. However, there is evidence suggesting that porous structures are robust against loads which are not taken into account in the optimization procedure (Torres et al., 2019). Therefore, it is an additional advantage that the final designs are porous. A fourth limitation pertains to the manufacturability of the final designs. The minimum strut size and the interconnectivity of the pores is not enforced by the TO formulation and can therefore not be ensured. A final limitation is that cell experiments to verify the SBSs biological performance are not performed in this study. However, we aimed the pore size ranges of the final designs to be suitable for bone in-growth based on recent literature. The authors believe that the full-scale topology optimization approach, upon further development, can become a good alternative for the currently used multi-scale topology optimization approaches for optimizing bone scaffolds as we show that the performance of the resulting scaffolds is expected to be better, and several disadvantages of the multi-scale approaches are solved.

5. Conclusions

This study investigated the application of full-scale topology optimization to design synthetic bone scaffolds with tuneable morphological and mechanical properties. The test problem indicates that the full-scale topology optimization approach increases the performance by 81% of the designs of porous synthetic bone scaffolds compared to the currently used multi-scale methods. Although the test problem is not directly comparable to the 3D problem formulation, it indicates that the full-
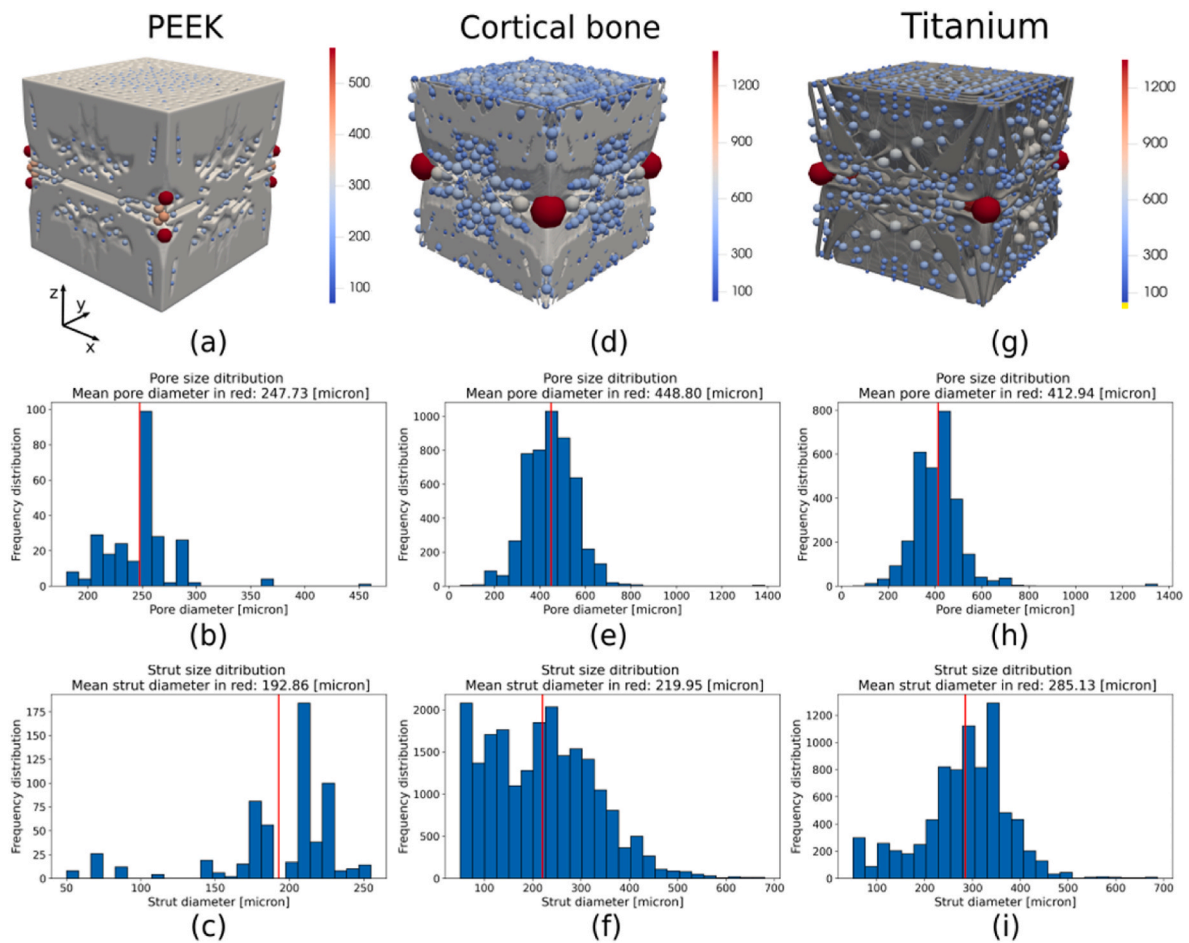
Fig. 6. Pore and strut diameter distributions for the PEEK (**a**), cortical bone (**d**) and titanium 3D designs (**g**). The resulting designs with the structures shown in grey and the size and colour of the spheres indicating the size of the pores. Histograms of the pore diameter distributions for PEEK (**b**), cortical bone (**e**) and titanium designs (**h**). Histograms of the strut diameter distributions for PEEK (**c**), cortical bone (**f**), and titanium designs (**i**).

Table 1
Constant parameters.

Symbol	Description	Value
ν	Poisson ratio	0.3
p	SIMP penalty	3.0
r	Density filter radius (no. elements)	2
x_0	Homogeneous initial condition	0.5

Table 2
3D scaffold mechanical and morphological properties.

Material	Description		Value	Unit
PEEK	Porosity		13.1	%
	Apparent elastic modulus	compression	1487.5	MPa
		shear in x	826.8	MPa
		shear in y	1125.0	MPa
Cortical bone	Porosity		85.8	%
	Apparent elastic modulus	compression	326.5	MPa
		shear in x	315.3	MPa
		shear in y	484.4	MPa
Titanium	Porosity		62.3	%
	Apparent elastic modulus	compression	937.5	MPa
		shear in x	1562.5	MPa
		shear in y	4687.5	MPa

scale topology optimization approach can eliminate the drawbacks of the multi-scale methods; fixed unit-cell geometry, the separation of scales assumption violation and the non-smooth transitions between unit-cells. The 2D parameter study reveals bone-like designs and a morphological-mechanical property relationship, similar to human vertebral trabecular bone. 3D designs are generated for PEEK, cortical bone, and titanium material properties where the PEEK and titanium designs are 3D-printed. The main limitation of the study is the extensive computational resources required to generate 3D designs. Furthermore, manufacturing constraints need to be explored as well as other applications need to be tested, in-silico and in-vivo. As the full-scale topology optimization approach for the design and optimization of bone scaffolds, is in the conceptual phase, more research should be done before we can assess its impact on clinical applications. With further development, the full-scale topology optimization approach would be an effective optimization approach for orthopaedic applications, which potentially provides superior design performance compared to the currently used multi-scale methods.

Funding

CRediT authorship contribution statement

Thijs Smit: Visualization, Validation, Software, Methodology, Investigation, Conceptualization, Writing – original draft. **Stijn Koppen:** Conceptualization. **Stephen J. Ferguson:** Funding acquisition.
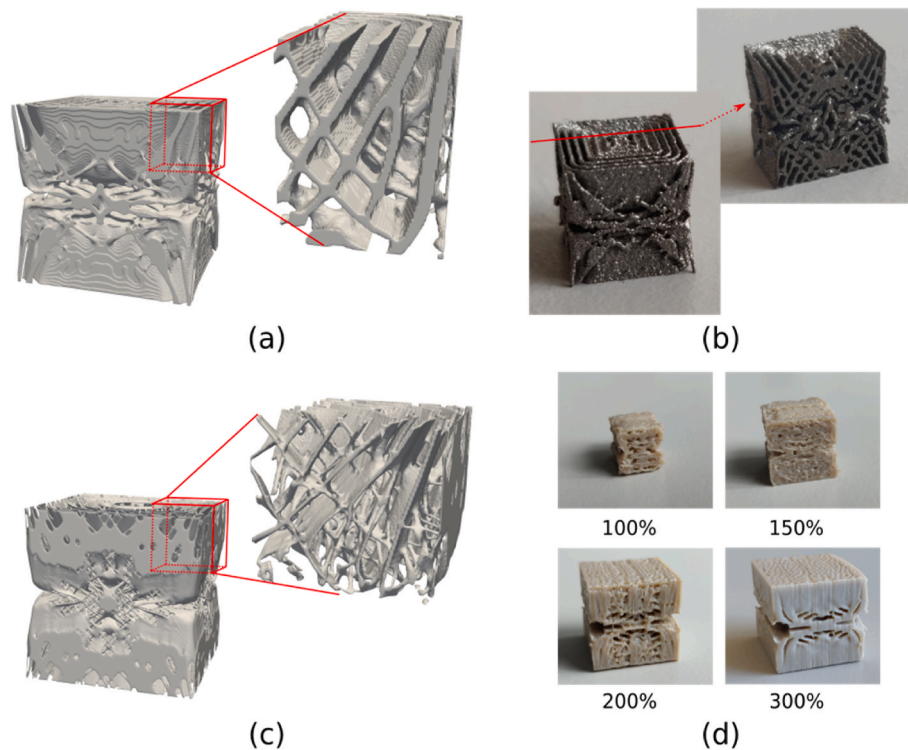
Fig. 7. 3D scaffold designs and cross-sections to visualize the porous internal structures (**a**) shows the titanium SBS design and a cross-section. The internal structure consists mostly of wall-like structures. (**b**) shows the 3D-printed titanium SBS and a cross-section. Wall-like structures are visible. (**c**) shows the 3D cortical bone design and cross-section exhibiting a few wall-like structures and many strut-like structures. (**d**) shows the 3D-Printed PEEK SBSs in 100%–300% scaling.

Benedikt Helgason: Supervision, Writing – review & editing.

Declaration of competing interest

Data availability

Data will be made available on request.

Acknowledgements

References

Aage, N., Andreassen, E., Lazarov, B.S., Sigmund, O., 2017. Giga-voxel computational morphogenesis for structural design. Nature 550, 84–86. https://doi.org/10.1038/nature23911.

Al-Tamimi, A.A., Fernandes, P.R.A., Peach, C., Cooper, G., Diver, C., Bartolo, P.J., 2017. Metallic bone fixation implants: a novel design approach for reducing the stress shielding phenomenon. Virtual Phys. Prototyp. 12, 141–151. https://doi.org/10.1080/17452759.2017.1307769.

Bahraminasab, M., 2020. Challenges on optimization of 3D-printed bone scaffolds. Biomed. Eng. Online 19, 1–33. https://doi.org/10.1186/s12938-020-00810-2.

Barba, D., Alabort, E., Reed, R.C., 2019. Synthetic bone: design by additive manufacturing. Acta Biomater. 97, 637–656. https://doi.org/10.1016/j.actbio.2019.07.049.

Boccaccio, A., Uva, A.E., Fiorentino, M., Lamberti, L., Monno, G., 2016. A mechanobiology-based algorithm to optimize the microstructure geometry of bone tissue scaffolds. Int. J. Biol. Sci. 12, 1–17. https://doi.org/10.7150/ijbs.13158.

Boerckel, J.D., Kolambkar, Y.M., Stevens, H.Y., Lin, A.S.P., Dupont, K.M., Guldberg, R.E., 2012. Effects of in vivo mechanical loading on large bone defect regeneration. J. Orthop. Res. 30, 1067–1075. https://doi.org/10.1002/jor.22042.

Bourdin, B., 2001. Filters in topology optimization. Int. J. Numer. Methods Eng. 50, 2143–2158. https://doi.org/10.1002/nme.116.

Carter, D.R., Blenman, P.R., Beaupré, G.S., 1988. Correlations between mechanical stress history and tissue differentiation in initial fracture healing. J. Orthop. Res. 6, 736–748. https://doi.org/10.1002/jor.1100060517.

Claes, L.E., Heigele, C.A., 1999. Magnitudes of local stress and strain along bony surfaces predict the course and type of fracture healing. J. Biomech. 32, 255–266.

Cohen, D.O., Aboutaleb, S.M.G., Johnson, A.W., Norato, J.A., 2021. Bone adaptation-driven design of periodic scaffolds. J. Mech. Des. Trans. ASME. 143, 1–16. https://doi.org/10.1115/1.4050928.

Du, Y., Liang, H., Xie, D., Mao, N., Zhao, J., Tian, Z., Wang, C., Shen, L., 2019. Finite element analysis of mechanical behavior, permeability of irregular porous scaffolds and lattice-based porous scaffolds. Mater. Res. Express 6. https://doi.org/10.1088/2053-1591/ab3ac1.

Egan, P.F., Gonella, V.C., Engensperger, M., Ferguson, S.J., Shea, K., 2017. Computationally designed lattices with tuned properties for tissue engineering using 3D printing. PLoS One 12, 1–20. https://doi.org/10.1371/journal.pone.0182902.

Egan, P., Wang, X., Greutert, H., Shea, K., Wuertz-Kozak, K., Ferguson, S., 2019. Mechanical and biological characterization of 3D printed lattices, 3D print. Addit. Manuf. 6, 73–81. https://doi.org/10.1089/3dp.2018.0125.

Gao, J., Luo, Z., Xia, L., Gao, L., 2019. Concurrent Topology Optimization of Multiscale Composite Structures in Matlab, Structural and Multidisciplinary Optimization. https://doi.org/10.1007/s00158-019-02323-6.

Garner, E., Kolken, H.M.A., Wang, C.C.L.L., Zadpoor, A.A., Wu, J., 2019. Compatibility in microstructural optimization for additive manufacturing. Addit. Manuf. 26, 65–75. https://doi.org/10.1016/j.addma.2018.12.007.

Garner, E., Wu, J., Zadpoor, A.A., 2022. Multi-objective design optimization of 3D micro-architected implants, Comput. Methods Appl. Mech. Eng. 396, 115102 https://doi.org/10.1016/j.cma.2022.115102.

Gostick, J., Aghighi, M., Hinebaugh, J., Tranter, T., Hoeh, M.A., Day, H., Spellacy, B., Sharqawy, M.H., Bazylak, A., Burns, A., Lehnert, W., Putz, A., 2016. OpenPNM: a pore network modeling package. Comput. Sci. Eng. 18, 60–74. https://doi.org/10.1109/MCSE.2016.49.

Gostick, J., Khan, Z., Tranter, T., Kok, M., Agnaou, M., Sadeghi, M., Jervis, R., 2019. PoreSpy: a Python toolkit for quantitative analysis of porous media images. J. Open Source Softw. 4, 1296. https://doi.org/10.21105/joss.01296.

Groen, J.P., Thomsen, C.R., Sigmund, O., 2021. Multi-scale topology optimization for stiffness and de-homogenization using implicit geometry modeling. Struct. Multidiscip. Optim. 63, 2919–2934. https://doi.org/10.1007/s00158-021-02874-7.

Guest, J.K., Pre, J.H., 2006. Optimizing multifunctional materials : Design of microstructures for maximized stiffness and fluid permeability. Int. J. Solid Struct. 43, 7028–7047. https://doi.org/10.1016/j.ijsolstr.2006.03.001.

Hollister, B.S.J., 2009. Scaffold Design and Manufacturing : from Concept to Clinic, pp. 3330–3342. https://doi.org/10.1002/adma.200802977.

Hollister, S.J., Maddox, R.D., Taboas, J.M., 2002. Optimal design and fabrication of scaffolds to mimic tissue properties. Biomaterials 23, 4095–4103.

Kelly, C.N., Sp, A., Eh, K., Shekhar, S., Walsh, W.R., Guldberg, R.E., Gall, K., 2021. Journal of the Mechanical Behavior of Biomedical Materials Functional repair of critically sized femoral defects treated with bioinspired titanium gyroid-sheet scaffolds. J. Mech. Behav. Biomed. Mater. 116, 104380 https://doi.org/10.1016/j.jmbbm.2021.104380.

Koppen, S., Langelaar, M., van Keulen, F., 2021. A simple and versatile topology optimization formulation for flexure synthesis. Mech. Mach. Theor. 172, 104743 https://doi.org/10.1016/j.mechmachtheory.2022.104743.

Melancon, D., Bagheri, Z.S., Johnston, R.B., Liu, L., Tanzer, M., Pasini, D., 2017. Mechanical characterization of structurally porous biomaterials built via additive manufacturing: experiments, predictive models, and design maps for load-bearing bone replacement implants. Acta Biomater. 63, 350–368. https://doi.org/10.1016/j.actbio.2017.09.013.

Metz, C., Duda, G.N., Checa, S., 2020. Towards multi-dynamic mechano-biological optimization of 3D-printed scaffolds to foster bone regeneration. Acta Biomater. 101, 117–127. https://doi.org/10.1016/j.actbio.2019.10.029.

J. Milovanović, M. Stojković, M. Trifunović, N. Vitković, Review of Bone Scaffold Design Concepts and Design Methods, Facta Univ. Ser. Mech. Eng. (n.d.).

Mittwede, P.N., Gottardi, R., Alexander, P.G., Tarkin, I.S., 2018. Rocky S. Tuan, Clinical Applications of Bone Tissue Engineering in Orthopedic Trauma, pp. 449–466. https://doi.org/10.1007/978-0-387-74660-9_15.

Mobbs, R.J., Coughlan, M., Thompson, R., Sutterlin, C.E., Phan, K., 2017. The utility of 3D printing for surgical planning and patient-specific implant design for complex spinal pathologies: case report. J. Neurosurg. Spine 26, 513–518. https://doi.org/10.3171/2016.9.SPINE16371.

Moussa, A., Rahman, S., Xu, M., Tanzer, M., Pasini, D., 2020. Topology optimization of 3D-printed structurally porous cage for acetabular reinforcement in total hip arthroplasty. J. Mech. Behav. Biomed. Mater. 105, 103705 https://doi.org/10.1016/j.jmbbm.2020.103705.

Pobloth, A.M., Checa, S., Razi, H., Petersen, A., Weaver, J.C., Chmidt-Bleek, K., Windolf, M., Tatai, A.A., Roth, C.P., Schaser, K.D., Duda, G.N., Schwabe, P., 2018. Mechanobiologically optimized 3D titanium-mesh scaffolds enhance bone regeneration in critical segmental defects in sheep. Sci. Transl. Med. 10 https://doi.org/10.1126/scitranslmed.aam8828.

Rincón-Kohli, L., Zysset, P.K., 2009. Multi-axial mechanical properties of human trabecular bone. Biomech. Model. Mechanobiol. 8, 195–208. https://doi.org/10.1007/s10237-008-0128-z.

Rohlmann, A., Graichen, F., Bender, A., Kayser, R., Bergmann, G., 2008. Loads on a telemeterized vertebral body replacement measured in three patients within the first postoperative month. Clin. Biomech. 23, 147–158. https://doi.org/10.1016/j.clinbiomech.2007.09.011.

Rubert, M., Vetsch, J.R., Lehtoviita, I., Sommer, M., Zhao, F., Studart, A.R., Müller, R., Hofmann, S., 2021. Scaffold pore geometry guides gene regulation and bone-like tissue formation in dynamic cultures. Tissue Eng. 00, 1–13. https://doi.org/10.1089/ten.tea.2020.0121.

Schroeder, W., Martin, K., Lorensen, B., 1996. The visualization toolkit: an object oriented approach to 3D graphics. Kitware Inc.pdf. In: J. Aust. Entomol. Soc., third ed., vol. 34, pp. 335–342.

Sigmund, O., Bendsøe, M.P., 2004. Topology Optimization.

Smit, T., Aage, N., Ferguson, S.J., Helgason, B., 2021. Topology optimization using PETSc: a Python wrapper and extended functionality. Struct. Multidiscip. Optim. 64, 4343–4353. https://doi.org/10.1007/s00158-021-03018-7.

Sutradhar, A., Paulino, G.H., Miller, M.J., Nguyen, T.H., 2010. Topological optimization for designing patient-specific large craniofacial segmental bone replacements. Proc. Natl. Acad. Sci. U. S. A 107, 13222–13227. https://doi.org/10.1073/pnas.1001208107.

Svanberg, K., 1987. The method of moving asymptotes—a new method for structural optimization. Int. J. Numer. Methods Eng. 24, 359–373. https://doi.org/10.1002/nme.1620240207.

Takahashi, H., 1982. An examination of the conformity of the orientation of bone trabeculae to the directions of principal stress in the case of the proximal end of the femur. J. Anthropol. Soc. Nippon 90, 53–60. https://doi.org/10.1537/ase1911.90.53.

Taniguchi, N., Fujibayashi, S., Takemoto, M., Sasaki, K., Otsuki, B., Nakamura, T., Matsushita, T., Kokubo, T., Matsuda, S., 2016. Effect of pore size on bone ingrowth into porous titanium implants fabricated by additive manufacturing: an in vivo experiment. Mater. Sci. Eng. C 59, 690–701. https://doi.org/10.1016/j.msec.2015.10.069.

Torres, A.M., Trikanad, A.A., Aubin, C.A., Lambers, F.M., Luna, M., Rimnac, C.M., Zavattieri, P., Hernandez, C.J., 2019. Bone-inspired microarchitectures achieve enhanced fatigue life. Proc. Natl. Acad. Sci. U. S. A 116, 24457–24462. https://doi.org/10.1073/pnas.1905814116.

van Oers, R.F.M., Ruimerman, R., Tanck, E., Hilbers, P.A.J., Huiskes, R., 2008. A unified theory for osteonal and hemi-osteonal remodeling. Bone 42, 250–259. https://doi.org/10.1016/j.bone.2007.10.009.

Vidal, L., Kampleitner, C., Krissian, S., Brennan, M., Hoffmann, O., Raymond, Y., Maazouz, Y., Ginebra, M.P., Rosset, P., Layrolle, P., 2020. Regeneration of segmental defects in metatarsus of sheep with vascularized and customized 3D-printed calcium phosphate scaffolds. Sci. Rep. 10, 1–11. https://doi.org/10.1038/s41598-020-63742-w.

von Doernberg, M.C., von Rechenberg, B., Bohner, M., Grünenfelder, S., van Lenthe, G. H., Müller, R., Gasser, B., Mathys, R., Baroud, G., Auer, J., 2006. In vivo behavior of calcium phosphate scaffolds with four different pore sizes. Biomaterials 27, 5186–5198. https://doi.org/10.1016/j.biomaterials.2006.05.051.

Wang, F., Stefanov, B., 2011. On Projection Methods, Convergence and Robust Formulations in Topology Optimization, pp. 767–784. https://doi.org/10.1007/s00158-010-0602-y.

Wang, X., Xu, S., Zhou, S., Xu, W., Leary, M., Choong, P., Qian, M., Brandt, M., Xie, Y.M., 2016. Topological design and additive manufacturing of porous metals for bone scaffolds and orthopaedic implants: a review. Biomaterials 83, 127–141. https://doi.org/10.1016/j.biomaterials.2016.01.012.

Wu, J., Aage, N., Westermann, R., Sigmund, O., 2018. Infill optimization for additive manufacturing-approaching bone-like porous structures. IEEE Trans. Vis. Comput. Graph. 24, 1127–1140. https://doi.org/10.1109/TVCG.2017.2655523.

Wu, J., Wang, W., Gao, X., 2019. Design and optimization of conforming lattice structures. IEEE Trans. Vis. Comput. Graph. https://doi.org/10.1109/tvcg.2019.2938946, 1–1.

Wu, C., Zheng, K., Fang, J., Steven, G.P., Li, Q., 2020. Time-dependent topology optimization of bone plates considering bone remodeling. Comput. Methods Appl. Mech. Eng. 359, 112702 https://doi.org/10.1016/j.cma.2019.112702.

Wu, J., Sigmund, O., Groen, J.P., 2021. Topology optimization of multi-scale structures: a review. Struct. Multidiscip. Optim. 63, 1455–1480. https://doi.org/10.1007/s00158-021-02881-8.

Zadpoor, A.A., 2019. Additively manufactured porous metallic biomaterials. J. Mater. Chem. B 7, 4088–4117. https://doi.org/10.1039/c9tb00420c.

Zhang, K., Cheng, G., 2022. Structural topology optimization with four additive manufacturing constraints by two-phase self-supporting design. Struct. Multidiscip. Optim. 65, 1–21. https://doi.org/10.1007/s00158-022-03366-y.

Zhang, W., Sun, S., 2006. Scale-related topology optimization of cellular materials and structures. Int. J. Numer. Methods Eng. 68, 993–1011. https://doi.org/10.1002/nme.1743.

Zhao, F., Li, D., Jin, Z., 2018. Preliminary investigation of poly-ether-ether-ketone based on fused deposition modeling for medical applications. Materials 11. https://doi.org/10.3390/ma11020288.

Zhou, B., Sherry Liu, X., Wang, J., Lucas Lu, X., Fields, A.J., Edward Guo, X., 2014. Dependence of mechanical properties of trabecular bone on plate-rod microstructure determined by individual trabecula segmentation (ITS). J. Biomech. 47, 702–708. https://doi.org/10.1016/j.jbiomech.2013.11.039.

Zysset, P.K., Edward Guo, X., Edward Hoffler, C., Moore, K.E., Goldstein, S.A., 1999. Elastic modulus and hardness of cortical and trabecular bone lamellae measured by nanoindentation in the human femur. J. Biomech. 32, 1005–1012. https://doi.org/10.1016/S0021-9290(99)00111-6.